Pion single-charge-exchange reactions above the Δ resonance

Naoko Nose-Togawa
Research Center for Nuclear Physics, Osaka University, Ibaraki 567-0047, Japan

Kenji Kume
Department of Physics, Nara Women's University, Nara 630-8506, Japan

(Received 17 March 2002; published 12 November 2002)

The pion single-charge-exchange reactions are studied for ^{13}C and ^{15}N above the delta resonance. The effect of the nuclear higher configurations is investigated for the cross section and the asymmetry under the distorted-wave impulse approximation. The cross section and the asymmetry are shown to be appreciably affected with the nuclear higher configurations.

DOI: 10.1103/PhysRevC.66.054603 PACS number(s): 25.80.Gn, 13.75.Gx, 21.60.Cs, 27.20.+n

Above the delta resonance, the pion-nucleon interaction becomes weaker than around the delta resonance, and the multiple scattering picture is believed to work well. Various pion-nucleus reactions have been studied both experimentally and theoretically [1–10]. Elastic scattering experiments have been carried out and are compared with the theory based on the Glauber or the optical-model description [1–8]. The Glauber and the optical-model calculations yield similar elastic cross sections which are smaller than experiments for ^{12}C and ^{40}Ca around the second peak [4–7]. The second-order effects or medium corrections are also studied but these corrections are not enough to explain the discrepancy between theory and experiment. The single-charge-exchange (SCX) reaction has been studied also above the delta resonance. Around the delta resonance, several authors showed the importance of the higher configurations for light nuclei [11–13]. Kamalov *et al.* [11] used the $2\hbar\omega$ component by Hicks *et al.* [14] which was slightly modified by Bennhold and Tiator [15] and have shown that the SCX cross sections are considerably affected by the admixture of the $2\hbar\omega$ component. Bennhold *et al.* [12] used the $(0+2)\hbar\omega$ shell-model wave function by Wolters *et al.* [16] for ^{15}N, which gives a narrower $M1$ form factor than the experiment. Bydzovsky *et al.* [13] also studied the (π^+,π^0) and (p,n) reactions on ^{13}C with the shell-model wave function by Wolters *et al.* [16]. To reproduce the experimental $M1$ form factor of ^{13}C, they replaced the spin-dependent part of the nuclear matrix element by a phenomenological $0\hbar\omega$ wave function by Tiator and Wright [17]. On the other hand, the core polarization is known to play an important role for the description of the $M1$ form factor for $0p$-shell nuclei [18–24]. For ^{13}C, the first-order core polarization is shown to enhance the isovector $[Y_0\otimes\sigma]$ component while little affects the $[Y_2\otimes\sigma]$ component. It considerably affects the isovector multipole densities for light nuclei. Then, the SCX cross section is expected to be sensitive to the nuclear higher configurations. Previously, we have studied the effect of core polarization on SCX around the delta resonance for ^{13}C and ^{15}N and have shown that it appreciably modifies the SCX observables [25].

Above the delta resonance, the spin-dependent pion-nucleon interaction becomes relatively larger around 750 MeV/c and we expect pronounced dependence of the SCX cross section and the asymmetry on nuclear structure. In the present work, we adopted the distorted-wave impulse approximation and examined the dependence of the SCX observables on nuclear higher configurations. The medium polarization effects for the forward SCX cross section were studied with somewhat different treatment for ^{14}C [26].

First, we describe the theoretical model used in the present work. The distorted-wave impulse approximation in momentum space is adopted to calculate the SCX amplitude. The pion-nucleus SCX amplitude for spin-$\frac{1}{2}$ nuclei leading to an isobaric analog state is given by

$$F=f(\theta)+ig(\theta)\boldsymbol{\sigma}\cdot(\hat{\mathbf{k}}_i\times\hat{\mathbf{k}}_f), \tag{1}$$

where $\boldsymbol{\sigma}$ is the spin operator of the target nucleus. The initial and the final pion momenta are denoted as $\mathbf{k}_i$ and $\mathbf{k}_f$, respectively. The differential cross section and the asymmetry are expressed as

$$\frac{d\sigma}{d\Omega}=|f(\theta)|^2+|g(\theta)|^2\sin^2\theta \tag{2}$$

and

$$A_y=\frac{2\,\mathrm{Im}(fg^*)\sin\theta}{|f(\theta)|^2+|g(\theta)|^2\sin^2\theta}. \tag{3}$$

The pion-nucleon scattering amplitude is decomposed into its partial-wave components

$$t(\mathbf{k}_i,\mathbf{k}_f:\omega)=\sum_\lambda\,[F_\lambda(k_0)P_\lambda(\cos\theta)+G_\lambda(k_0)i\boldsymbol{\sigma}\cdot(\hat{\mathbf{k}}_i\times\hat{\mathbf{k}}_f)P'_\lambda(\cos\theta)], \tag{4}$$

where k_0 is the on-shell momentum corresponding to the pion energy ω. We adopt the pion-nucleon phase shifts taken from the database SAID [27] and retain the partial waves up to $\lambda=6$ and assume the off-shell extrapolation of the pion-nucleon amplitude

$$F_\lambda(k_0)\rightarrow F_\lambda(k,k':\omega)=F_\lambda(k_0)g_\lambda(k)g_\lambda(k'), \tag{5}$$

and the same for $G_\lambda(k_0)$ with the Gaussian-type form factor

$$g_\lambda(k)=\left(\frac{k}{k_0}\right)^\lambda \exp\left[-\left(\frac{k-k_0}{\Lambda}\right)^2\right]. \tag{6}$$

Under the distorted-wave impulse approximation, the non-spin-flip and the spin-flip pion-nucleus SCX amplitudes are expressed as

$$\begin{aligned}f(\theta)=&\frac{1}{2\sqrt{6\pi}}\sum_\ell (2\ell+1)P_\ell(\cos\theta)\sum_{\lambda,\ell_1}\frac{2\ell_1+1}{2\lambda+1}F_\lambda(k_0)\\&\times(\ell\ell_1 00|\lambda 0)^2\int r^2dr\left[\int j_{\ell_1}(kr)\phi_\ell^{(f)}(k)g_\lambda(k)k^2dk\right]^*\\&\times\left[\int j_{\ell_1}(k'r)\phi_\ell^{(i)}(k')g_\lambda(k')k'^2dk'\right]F_{000}(r)\end{aligned} \tag{7}$$

and

$$\begin{aligned}g(\theta)=&\frac{1}{2\sqrt{6\pi}}\sum_\ell (-)^\ell(2\ell+1)P'_\ell(\cos\theta)\sum_{\lambda,\ell_1,\ell_2,L}\\&\times\sqrt{\frac{(2\ell+1)\lambda(\lambda+1)(2\lambda+1)(2\ell_1+1)(2\ell_2+1)}{\ell(\ell+1)}}\\&\times G_\lambda(k_0)(-)^\lambda(\lambda\ell 00|\ell_1 0)(\lambda\ell 00|\ell_2 0)\\&\times(\ell_1\ell_2 00|L0)i^{\ell_1-\ell_2}\int r^2dr\\&\times\left[\int j_{\ell_2}(kr)\phi_\ell^{(f)}(k)g_\lambda(k)k^2dk\right]^*\\&\times\left[\int j_{\ell_1}(k'r)\phi_\ell^{(i)}(k')g_\lambda(k')k'^2dk'\right]\\&\times\begin{Bmatrix}\ell_1 & \lambda & \ell\\ \ell_2 & \lambda & \ell\\ L & 1 & 1\end{Bmatrix}F_{L11}(r),\end{aligned} \tag{8}$$

where $\phi_\ell^{(i)}(k)$ and $\phi_\ell^{(f)}(k)$ are the initial and the final pion radial wave functions in momentum space. $F_{LSJ}(r)$ is the isovector nuclear transition density defined as the spin and the isospin reduced nuclear matrix element of the operator $\hat{O}_{LSJ}$,

$$F_{LSJ}(r)=\langle f||\hat{O}_{LSJ}||i\rangle, \tag{9}$$

with

$$\hat{O}_{LSJ}=\sum_j [Y_L(\hat{\mathbf{r}}_j)\otimes\sigma_j^{(S)}]^J\frac{\delta(r-r_j)}{r^2}\tau_j. \tag{10}$$

The pion distorted waves are generated by the first-order pion-nucleus optical potential as

$$\langle\mathbf{k}'|V_{\rm opt}|\mathbf{k}\rangle\simeq\frac{A-1}{A}\rho(\mathbf{q})\langle\mathbf{k}'\mathbf{p}'|t|\mathbf{kp}\rangle, \tag{11}$$

where $\mathbf{q}=\mathbf{k}'-\mathbf{k}$. $\mathbf{k}$ and $\mathbf{p}$ are the pion and the nucleon momenta in the pion-nucleus center-of-mass system. By neglecting the nucleon Fermi motion in the nucleus, we fix the nucleon momenta to be $\mathbf{p}=-\mathbf{k}/A$ and $\mathbf{p}'=-\mathbf{k}'/A$ and the optical potential can be expressed as

$$\langle\mathbf{k}'|V_{\rm opt}|\mathbf{k}\rangle\simeq\frac{A-1}{A}\rho(\mathbf{q})\Gamma\langle\boldsymbol{\kappa}'|t|\boldsymbol{\kappa}\rangle, \tag{12}$$

where $\boldsymbol{\kappa}$ and $\boldsymbol{\kappa}'$ are the pion momenta in the pion-nucleon center-of-mass frame and the kinematical transformation factor Γ is given by

$$\Gamma=\left[\frac{\omega(\kappa)\omega(\kappa')E(\kappa)E(\kappa')}{\omega(k)\omega(k')E\left(\frac{k}{A}\right)E\left(\frac{k'}{A}\right)}\right]^{1/2}, \tag{13}$$

with the pion and the nucleon energies

$$\omega(\kappa)=\sqrt{\kappa^2+\mu^2} \tag{14}$$

and

$$E(\kappa)=\sqrt{\kappa^2+M^2}. \tag{15}$$

In above equation, we neglected the angle transformation from pion-nucleon to pion-nucleus center-of-mass frames. By taking into account the non-spin-flip term in Eq. (4), the partial wave decomposition of the optical potential is straightforward and we obtain

$$V_\ell^{\rm opt}=\frac{4\pi}{2\ell+1}\sum_{\lambda,\ell'}F_\lambda(k,k':\omega)(\lambda\ell' 00|\ell 0)^2\rho_{\ell'}(k,k'), \tag{16}$$

where $\rho_{l'}(k,k')$ is the coefficient of the multipole expansion of the nuclear density $\rho(r)$,

$$\int e^{-i\mathbf{k}'\cdot\mathbf{r}}\rho(r)e^{i\mathbf{k}\cdot\mathbf{r}}d\mathbf{r}=\sum_\ell \rho_\ell(k,k')P_l(\cos\theta). \tag{17}$$

The pion-nucleus distorted waves are calculated by the Klein-Gordon equation in momentum space:

$$(k_0^2-k^2)\phi_l(k)=2\omega\int V_l^{\rm opt}(k,k')\phi_l(k')k'^2dk'. \tag{18}$$

The above equation is discretized and the conventional matrix inversion method is used to solve the integral equation. For the cutoff mass in Eq. (6), we take $\Lambda=0.8$ GeV which was used in the analysis of the pion-nucleon elastic scattering [28]. Since the experimental data for ^{13}C and ^{15}N are not available, we have compared the theoretical elastic scattering cross section with the experiment for π^--^{12}C. In Fig. 1, the solid line is the result at the pion momentum $p_\pi=790$ MeV/c. As is known, the first-order calculation underestimates the experimental data around the second dip. Several possible corrections such as the pion absorption and the second-order effect are estimated but still there remains the discrepancy between theory and experiment at these en-

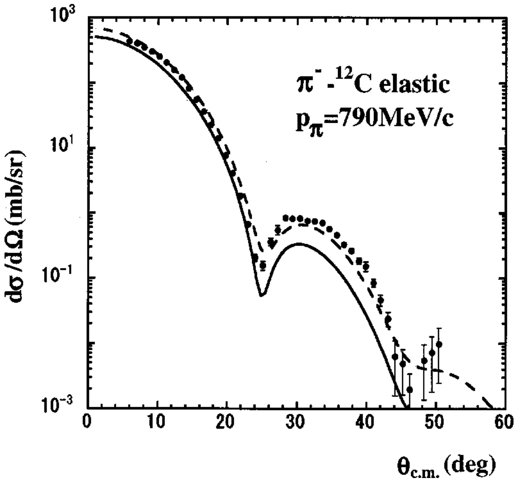

FIG. 1. π^--^{12}C elastic scattering cross section at the pion momentum $p_\pi = 790$ MeV/c. The solid line is the result with the first-order optical potential in Eq. (16). The dashed line is the result calculated by modifying the pion-nucleon t matrix $t \rightarrow s_R t_R + i s_I t_I$ as described in the text with $s_R = 1.65$ and $s_I = 1.20$. The experimental data are taken from Ref. [32].

ergy regions. To see the effect on the SCX cross sections, we simply modified the real and the imaginary parts of the pion-nucleon t matrix separately as

$$t(\mathbf{k}_i,\mathbf{k}_f:\omega) \rightarrow s_R t_R(\mathbf{k}_i,\mathbf{k}_f:\omega) + i s_I t_I(\mathbf{k}_i,\mathbf{k}_f:\omega), \quad (19)$$

and the parameters s_R and s_I are varied to fit the experimental elastic cross sections for π^--^{12}C. We obtained $s_R = 1.65$ and $s_I = 1.20$ with $b = 1.583$ fm and the elastic cross section is shown as a dashed curve in Fig. 1. The SCX amplitudes are calculated with Eqs. (7) and (8). The isovector nuclear transition density relevant to the SCX process is calculated with a Cohen-Kurath $0p$-shell-model wave function with the two-body matrix element (8–16) POT [29]. We take the oscillator parameter $b = 1.543$ fm for ^{13}C and $b = 1.67$ fm for ^{15}N. The effect of the core polarization is calculated under the first-order perturbation

$$F_{LSJ}(r) = \langle f || \hat{O}_{LSJ} || i \rangle + \left\langle f \left|\left| \hat{O}_{LSJ} \frac{1}{E_f - H_0}(V_{\mathrm{res}} - U) \right|\right| i \right\rangle + \left\langle f \left|\left| (V_{\mathrm{res}} - U) \frac{1}{E_i - H_0} \hat{O}_{LSJ} \right|\right| i \right\rangle, \quad (20)$$

where V_{res} is a two-body residual interaction, and the one-body Hartree-Fock contribution U is subtracted which is important for open-shell nuclei [24]. As a central part of the residual interaction, we adopt the Yukawa form with the Rosenfeld mixture [24] or the $M3Y$ interaction [30]. As a noncentral part, we adopt the tensor force of Hamada-Johnstone nucleon-nucleon interaction [31] with the cutoff radius $r_c = 0.7$ fm. As the intermediate states we included the configurations up to $12\hbar\omega$ excitation energies. The SCX cross sections for ^{13}C$(\pi^+,\pi^0)^{13}$N$_{IAS}$ at $p_\pi = 800$ MeV/c are

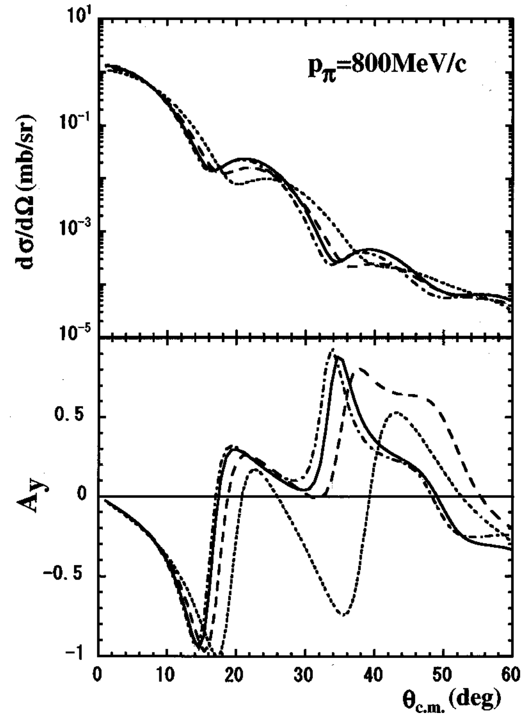

FIG. 2. The cross section and the asymmetry for the SCX reaction ^{13}C$(\pi^+,\pi^0)^{13}$N$_{IAS}$ at $p_\pi = 800$ MeV/c. The dotted lines are the results with the Cohen-Kurath wave function. The results are also shown including the core polarization effects with the Rosenfeld (solid lines) and $M3Y$ (dashed lines) interactions. The dot-dashed lines are calculated with the Rosenfeld force and the oscillator parameter $b = 1.6$ fm.

shown in Fig. 2. The dotted line is the result with the $0p$-shell-model wave function without higher configurations. The solid and the dashed lines are the results including the core polarization effects using the isovector density calculated in Eq. (20) with the Rosenfeld-type and the $M3Y$ residual interactions, respectively. Both are calculated with the oscillator parameter $b = 1.543$ fm which well describes the $M1$ form factor of ^{13}C. The isovector transition density F_{000} gives the dominant contribution and the core polarization reduces the overall magnitude of this density while slightly shifting it to the outward direction. Because of this, the SCX cross section is shifted to the forward direction by the core polarization. This is almost the same for the angular distribution of the asymmetry. Due to the nuclear absorption, the SCX cross section is expected to be sensitive to the transition density around the nuclear surface. To see the sensitivity, we calculated the cross section using the oscillator parameter $b = 1.6$ fm with the Rosenfeld exchange mixture as the dash-dotted line in Fig. 2. The angular distribution is only slightly shifted to the forward direction. At the forward region $\theta \leqslant 30°$ the results with the higher configurations are almost the same and are not strongly dependent on the choice of the residual interactions. In Fig. 3, the cross section and the asymmetry for the reaction ^{13}C$(\pi^+,\pi^0)^{13}N_{IAS}$ are shown at incident pion momenta 600, 800, and 1000 MeV/c. The long-dashed lines are the results with the $0p$-shell Cohen-Kurath wave function while the solid lines are with the core polar-

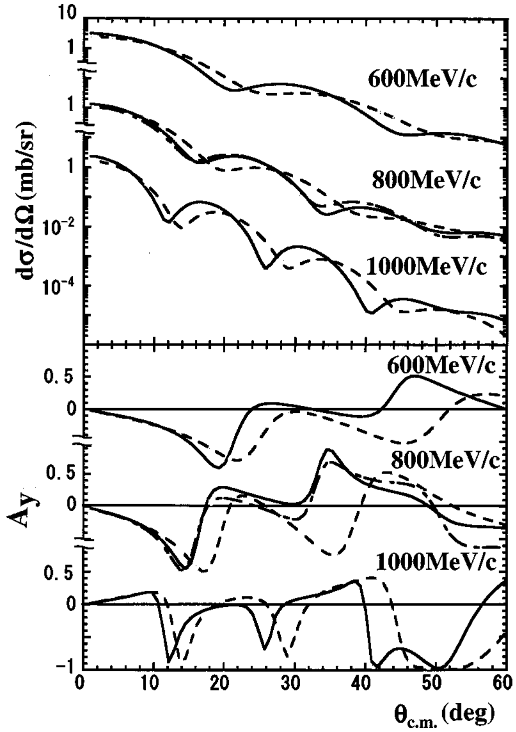

FIG. 3. The cross section and the asymmetry for the SCX reaction $^{13}C(\pi^+,\pi^0)^{13}N_{IAS}$ at several incident pion momenta. The long-dashed lines are calculated with the $0p$-shell Cohen-Kurath wave function, while the solid lines correspond to the results including the core polarization with the Rosenfeld exchange mixture. For the incident momentum $p_\pi=800$ MeV/c, the dash-dotted lines are the results by the pion distorted wave calculated with the modified pion-nucleon t matrix described in the text.

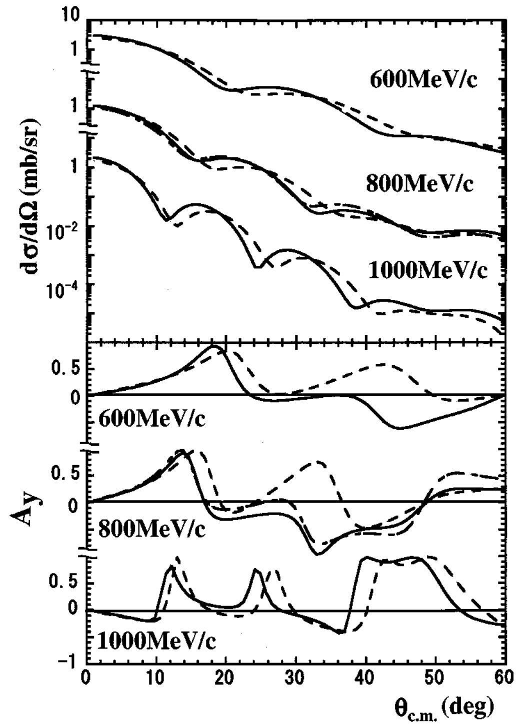

FIG. 4. The same as in Fig. 3, but for the SCX reaction $^{15}N(\pi^+,\pi^0)^{15}O_{IAS}$ at various incident pion momenta.

ization calculated by the Rosenfeld force with $b=1.543$ fm. The trends for the cross sections are almost the same for various incident energies. The asymmetry at the forward direction changes its sign for the incident momentum 1000 MeV/c. For the case of the incident momentum 800 MeV/c, the dash-dotted lines are the results with the pion-nucleon t matrix modified to fit the elastic cross section for ^{12}C at 790 MeV/c as shown in Fig. 1. The influence of the pion distorted waves which gives a fairly different elastic cross section is quite small for the SCX cross section and the asymmetry. We also examined the various dependencies of the SCX cross section for the input parameters. We used another form of the cutoff function

$$g_\lambda(k)=\left(\frac{k}{k_0}\right)^\lambda \frac{1}{1+\left(\dfrac{k-k_0}{\Lambda}\right)^2} \tag{21}$$

with $\Lambda=0.8$ GeV. The modification of the off-shell part of the pion-nucleon amplitude slightly affects the SCX cross section only around the first and the second dips. For the asymmetry, the different off-shell model gives basically the similar oscillatory structure of the asymmetry but the peak height is slightly changed by about 0.1–0.2. We also calculated the SCX cross section with the Woods-Saxon-type single-particle wave functions. The results are almost the same as those with the harmonic-oscillator wave functions for the cross section and we cannot distinguish the difference in the figure. For the asymmetry, both calculations give slightly different results only at $\theta>45°$. Thus these input parameter dependencies are not large and do not influence the present discussions. In Fig. 4, we show the results for the reaction $^{15}N(\pi^+,\pi^0)^{15}O_{IAS}$ at various incident momenta. The core polarization effects are almost the same as those for ^{13}C. It is interesting to note that the asymmetry has the opposite sign to those for ^{13}C. This is due to the fact that the dominant configuration for ^{13}C is the $0p_{1/2}$ neutron particle while for ^{15}N, it is $0p_{1/2}$ proton hole states. This gives the opposite sign for the isovector spin-dependent transition density F_{011} for these nuclei.

Above the delta resonance, the pion-nucleon interaction becomes weaker than around the delta resonance, and the multiple scattering picture is believed to work well. Thus, the various nuclear effects are expected to be seen clearly. In the present paper, we have studied the effect of nuclear higher configurations for SCX reactions on ^{13}C and ^{15}N above the delta resonance region. The core polarization moderately influences the cross section and the asymmetry, especially around 800 MeV/c. The angular distributions are shifted to the forward direction. These results are not sensitive to the choice of the two-body residual interaction. The first-order pion-nucleus potential and the modified optical potential, which fits the elastic cross section, give similar results for the SCX observables. The present results indicate that the effects of the nuclear configurations are important for the quantitative study of the SCX reaction.

[1] M. Mizoguchi, K. Sumiyoshi, T. Kajino, and H. Toki, Prog. Theor. Phys. **81**, 1217 (1989).
[2] V. Franco and H.G. Schlaile, Phys. Rev. C **41**, 1075 (1990).
[3] M. Mizoguchi and H. Toki, Nucl. Phys. **A513**, 685 (1990).
[4] E. Oset and D. Strottman, Phys. Rev. C **44**, 468 (1991).
[5] M. Arima, K. Masutani, and R. Seki, Phys. Rev. C **44**, 415 (1991).
[6] M. Arima, K. Masutani, and R. Seki, Phys. Rev. C **51**, 285 (1995).
[7] M. Arima, K. Masutani, and R. Seki, Phys. Rev. C **51**, 431 (1995).
[8] D. Marlow *et al.*, Phys. Rev. C **30**, 1662 (1984).
[9] A.L. Williams *et al.*, Phys. Lett. B **216**, 11 (1989).
[10] E. Oset and D. Strottman, Phys. Rev. Lett. **70**, 146 (1993).
[11] S.S. Kamalov, C. Bennhold, and R. Mach, Phys. Lett. B **259**, 410 (1991).
[12] C. Bennhold, L. Tiator, S.S. Kamalov, and R. Mach, Phys. Rev. C **46**, 2456 (1992).
[13] P. Bydzovsky, R. Mach, and S.S. Kamalov, Nucl. Phys. **A574**, 685 (1994).
[14] R.S. Hicks, J. Dubach, R.A. Lindgren, B. Parker, and G.A. Peterson, Phys. Rev. C **26**, 339 (1982).
[15] C. Bennhold and L. Tiator, Phys. Lett. B **238**, 31 (1990).
[16] A.A. Wolters, A.G.M. van Hees, and P.W.G. Glaudemans, Phys. Rev. C **42**, 2053 (1990); **42**, 2062 (1990).
[17] L. Tiator and L.E. Wright, Phys. Rev. C **30**, 989 (1984).
[18] H. Toki and W. Weise, Phys. Lett. **92B**, 265 (1980).
[19] J. Delorme, M. Ericson, A. Figureau, and N. Giraud, Phys. Lett. **92B**, 327 (1980).
[20] J. Delorme, A. Figureau, and P. Guichon, Phys. Lett. **99B**, 187 (1981).
[21] T. Suzuki, F. Osterfeld, and J. Speth, Phys. Lett. **100B**, 443 (1981).
[22] H. Sagawa, T. Suzuki, H. Hyuga, and A. Arima, Nucl. Phys. **A322**, 361 (1979).
[23] T. Suzuki, H. Hyuga, A. Arima, and K. Yazaki, Nucl. Phys. **A358**, 421 (1981).
[24] T. Suzuki, H. Hyuga, A. Arima, and K. Yazaki, Phys. Lett. **106B**, 19 (1981).
[25] N. Nose and K. Kume, Phys. Rev. C **54**, 432 (1996).
[26] E. Oset, D. Strottman, H. Toki, and J. Navarro, Phys. Rev. C **48**, 2395 (1993).
[27] R.A. Arndt *et al.*, Phys. Rev. D **43**, 2131 (1991).
[28] R.A. Eisenstein and F. Tabakin, Comput. Phys. Commun. **12**, 237 (1976).
[29] S. Cohen and K. Kurath, Nucl. Phys. **73**, 1 (1965).
[30] G. Bertsch, J. Borysowicz, H. McManus, and W.G. Love, Nucl. Phys. **A284**, 399 (1977).
[31] T. Hamada and I.D. Johnstone, Nucl. Phys. **34**, 382 (1962).
[32] T. Takahashi *et al.*, Phys. Rev. C **51**, 2542 (1995).